Methods for Evaluating Particle Coalescence and their Implications in Laser Sintering

L. Benedetti*[a], B. Brulé[b], N. Decraemer[b], K. E. Evans[a], O. Ghita[a]

[a] *University of Exeter, College of Engineering, Mathematics and Physical Sciences, EX4 4QF Exeter, United Kingdom*
[b] *Arkema, Cerdato, Route du Rilsan, 27470 Serquigny, France*

Abstract

An experimental study on the melt and coalescence of different Poly(aryl ether ketones) (PAEK) powders was carried out. The study consisted of evaluating individual particles and neck growth using a hot stage platform. Three different methods of assessing particles dimensions were evaluated, and the coalescence was compared for the grades on three different substrates: glass, glass coated silicone and on amorphous PEKK films, the last substrate with the intent to relate with the laser sintering process. It was found that all individual particles shrink prior to melting, achieving up to 30% reduction in perimeter at temperatures just above melting. This shrinkage is followed by an increase in size, mostly driven by viscous flow. The shrinkage seems to affect neck growth by delaying coalescence, as particles are pulled away whilst neck increases. This is a plausible explanation for why neck growth occurs at a lower rate than predicted by most coalescence models. The methods using Feret diameter and perimeter are quite accurate, whilst the use of different substrates do not seem to affect particle coalescence or change in dimension. Viscosity and particle size influence overall particle behaviour and melt, whilst morphology and porosity do not have a great impact in particle coalescence.

Keywords:

Laser Sintering, Coalescence, PEKK, PEEK, High Temperature.

*Corresponding author.
Telephone number: +44 (0) 1392 725 831
E-mail address: lb636@exeter.ac.uk

Nomenclature

List of Symbols

T_m Temperature of melting

T_g Glass transition temperature

D Ratio of particle size at a specific temperature x by particle size at room temperature i

Y Ratio of length of contact between two particles at a specific temperature x by length of contact of these particles at room temperature i

y neck length

d_i Diameter at room temperature

d_f Feret diameter

p Perimeter

1. Introduction

Laser Sintering (LS) is a powder bed technology which produces 3D parts by applying successive layers of powder on the top of each other. Each layer deposition is followed by the application of thermal energy supplied by a laser beam to solidify the areas described by the Computer Aided Design (CAD) representation. The powders suitable for LS require several specific characteristics often not well understood and complicated to achieve. Ideally, spherical morphology is preferred to improve flow and increase packing efficiency [1–6]. Particle size and distribution seem to significantly affect packing efficiency and final part consolidation. Yang & Evans [5] and Amado et al. [4] suggest a narrow distribution around 60μm and a small amount of fine particles at 10μm for polymer powders. Particle density is also important to guarantee sintered parts with higher density, dimensional accuracy and strength. However it may compromise flow properties [7].

Other properties suitable for good laser sintering concern rheological behaviour. Viscosity must be low enough to promote consolidation, but not too low to compromise mechanical performance and cause high shrinkage and poor dimensional accuracy [8, 9]. Surface tension is another fundamental parameter to understand particle coalescence and growth and it helps determining the success of sintering [8, 10]. For semicrystalline polymers, laser sintering occurs when the polymer is heated above $\mathrm{T_m}$, promoting the rapid change into a viscous liquid. However, due to the short time of laser exposure, the melting process is still driven by the coalescence of particles at bed temperature [11], therefore the pre-heating and post-heating of the powder just below $\mathrm{T_m}$ is important as well to guarantee full consolidation throughout manufacturing and prevent major shrinkage [12].

The role of coalescence is fundamental to understanding the consolidation mechanism of laser sintered parts [13–16]. The first study was proposed by Frenkel [17] in 1945 and soon modified by Eshelby, Mackenzie

& Shuttleworth in 1949 [18]. Their study focused on the behaviour of viscous flow under the action of surface tension. The Frenkel-Eshelby model provides a general approximation to the experimental results achieved in recent literature and is widely used to understand the parameters influencing the process of coalescence. This model is presented in Equation 1.

$$\frac{y}{r} = \left(\frac{\Gamma t}{\eta_0}\right)^{1/2} \tag{1}$$

In which y is the half neck radius, r is the particle radius, Γ is the surface tension, η_0 is the zero-shear viscosity and t is time. According to this model, coalescence is completed at y/d_i close to 1.26. However, Frenkel and Eshelby considered two spherical particles with the same size and no thermal gradient within the particles [19], as represented in Figure 1. Hopper [20] proposed a coalescence model for two equal cylinders instead, driven by capillary forces. He used Navier-Stokes equations for two dimensional viscous flow and found coalescence is completed at y/d_i equals to 1.41 [21]. This difference in values highlights the importance of assessing particle shape when measuring rate of coalescence.

Bellehumeur et al. [22] applied both models described to compare the effect of coalescence on different grades of polyethylene. They concluded that the model proposed by Hopper represents better the coalescence process than Frenkel-Eshelby model, although both showed higher values of coalescence rate if compared with their experimental data for polyethylene grades. They also claimed that Frenkel model considers particle radius constant with temperature, and such assumption is only satisfactory for y/d_i lower than 0.3. Hence, Pokluda et al. [21] proposed a different model which accounts for the variation of particle radius with time during the coalescence process. None of these models, however, consider viscoelastic effects, the adhesion forces between particles and the effect of the sintering surface, which may not be negligible.

The coalescence of polymers differ from other classes of materials as polymer melts exhibit complex viscoelastic properties over a wider range of time and temperature [23]. Kuczynski et al. [24] and Mazur & Plazek [23] showed that coalescence of acrylic resins has a viscoelastic response, hence Newtonian sintering models are not applicable and predict faster coalescence rates than observed. Jagota et al. [25] separated the viscoelastic behaviour of particles into initial elastic adhesion and viscous sintering. They mention two different modes of contact growth driven by surface forces: the first is known as initial elastic contact, it is predominant in the early stage of sintering and is dominated by van der Waals attraction forces acting in a zipping mode contact closure across the gap ahead of the contact edge (Figure 2(a)). In the later stage, curvature-based tractions normal to the surface of the sphere drive viscous sintering, and the contact grows in a stretching mode (Figure 2(b)). The transition between both modes is therefore viscoelastic and dependent on the contact radius, hence dependent on particle radius.

For Mazur & Plazek [23], coalescence in polymers is delayed, among other reasons, by the diffusion of chains across the interface and the establishment of an equilibrium distribution of chain entanglements. As

Jagota et al. [25], they also studied acrylic and found that stress relaxation occurs regardless of particle size. Therefore, time for chain relaxation must be taken into account to obtain bulk mechanical properties. Bellehumer et al. [26] used Frenkel-Eshelby model with Pokluda assumption but also considering viscoelastic effects to study sintering of different grades of polyethylene and propylene ethylene copolymers. They concluded that sintering is slower for more elastic polymers as well as the action of surface tension is best described when using Maxwell model in Frenkel's equation.

To track particle coalescence experimentally, several studies have used Hot Stage Microscopy (HSM) pictures [13, 19, 27, 28] and successfully measured neck growth between polymer particles. Barnetson and Hornsby, [29], however, mention a few limitations of this technique: the substrate, i.e. glass plates, can act as a barrier to heat transfer in different degrees according to the contact surface of the particle to the substrate, and the difficulty in visualizing whether the particles are only touching or overlapping each other. Although a drawback for all HSM evaluations, no study proposed an experimental solution for the influence of different contact areas of the particles with the substrate. Furthermore, no substrate other than glass was evaluated in order to understand better the coalescence process or compare with manufacturing techniques, such as powder bed sintering, in which a layer of partially molten powder is just below a layer of solid particles ready for sintering.

This paper discusses methods for evaluating particles coalescence and aims to understand and correlate particle characteristics with final consolidation in the laser sintering process. To support the comparison with the LS process, the effect of different substrates was evaluated, including a substrate from the same material as the powder grades on the top. This is the first study which investigates the effect of different substrates in HSM and the first study to evaluate individual particles changing in shape and size prior to their neck formation and growth.

2. Experimental

2.1. Materials

The experiments were conducted with HP3, a poly(ether ketone) (PEK) supplied by EOS E-Manufacturing Solutions [30], and three other non-commercially available poly(ether ketone ketone) (PEKK) polymers supplied by Arkema Innovative Chemistry and referenced as PEKK 6000 series [31]. These polymers were prepared with the concentration of 60/40 T/I of terephthalic acid (T) with para phenyl links and isophthalic acid (I) with meta phenyl links [31, 32]. The viscosity, glass transition temperature (T_g) and melting temperature (T_m) of each grade are listed in Table 1.

The non-commercially available grades, HL1316, P12S959a and HL1320 PEKK, will be referred in this study as, respectively, A1, A2 and B1 polymers.

2.2. Scanning Electron Microscopy

Scanning Electron Microscopy (SEM) analysis was performed using a Hitachi S-3200N scanning electron microscope. The accelerating voltage and the current selected were, respectively, 10kV and 0.13nA. The samples were coated with 10nm thick of gold and images at magnitudes of 1000 and 3500 times were captured.

2.3. Particle Size Distribution

Particle Size and Distribution (PSD) test was performed using a Malvern Mastersizer 3000E laser diffraction equipment. A small sample of powder was dispersed at room temperature in a liquid solution of 0.4% of sodium hexametaphosphate to prevent the stabilization of bubbles while measuring particle size. The test was repeated three times for each sample, with five measurements collected at each repeat.

2.4. Powder Rheology and Flowability

A Freeman FT-4 powder Rheometer was used to assess powder flow properties and the effect of powder morphology on overall performance. Four parameters were analysed; a brief description of them is found in Table 2.

The test was performed in a 25ml split vessel filled with powder in a pre-conditioned state, which involves a gentle displacement of the sample to loose and slightly aerate the powder, therefore removing any pre-compaction or excess of air. The conditioned bulk density (CBD) is measured at this stage, in which any external effect can be neglected and the volume is constrained to 25ml. The blade applies a torque by rotating counter-clockwise at 100mm/s whilst moving downwards. In the standard methodology, such movement is repeated seven times; the average energy required to perform one rotation at the last repeat divided by the average energy required to perform one rotation in the first repeat is known as the stability index (SI). The Basic Flowability Energy (BFE) is measured in the last cycle of the blade rotating counter-clockwise at 100mm/s, which is, applying pressure to the system. The Specific Energy (SE) is calculated by performing the average of energy applied to lift the blade by rotating it clockwise at the last and second last rotation of test at 100mm/s; the average is divided by the mass contained in the vessel so that the effect of powder packing is negligible [33].

An ideal powder regarding flow properties would have an SI value as close to 1 as possible, a high CBD, high BFE and low SE, therefore suggesting a uniform packing and a free-flow behaviour. To compare the difference in the SI for each material, the number of repeats were increased until a plateau is reached. This plateau varies according to the grade in analysis, hence the number of repeats was adjusted accordingly.

2.5. Hot Stage Microscopy Analysis

To analyse particle coalescence with the intent to predict such phenomena in the Laser Sintering system, Hot Stage Microscopy (HSM) was performed. This test aims to understand individual particle behaviour

with temperature increase, the effect of morphology during the process of heating and melting and compare different substrates and their effect in the coalescence process. Three substrates were used in this study: glass slides, glass slides coated with silicone and PEKK films on glass slides.

Glass slides are the standard substrate used to perform HSM and most experiments described in literature used glass as a substrate [11, 28, 34, 35]. To prevent particles wetting on glass slides, a silicone-based separator spray was used as coating. A fine layer was gently sprayed on each glass slide and they were left to dry for a minimum of one day. Finally, the coalescence behaviour was also tracked on top of 100 μm thick films of PEKK provided by Arkema, from 6000 series. The film was placed just above the glass slides.

The test was performed in a Linkam THMS600 microscope stage coupled with a Bruker IRScope II and connected to a DinoEye eyepiece camera. The IRScope operated in reflection mode and in the range of visual spectrum, at a magnification of 400 times. To simulate better the LS process, the test was performed dynamically from room temperature to a maximum of 450 °C, at 120 °C x min^{-1}. The pictures were captured every 2s, hence in an interval of 4 °C per picture, with the assistance of DinoCapture 2.0 software.

The analysis was performed using ImageJ software. A total of 20 pictures were selected for each trial, starting from the image in which neck is formed. Such image is different for each grade as T_m is different (Table 1) and it varies slightly for each experiment. The selection of this image was based on change in brightness of the particles; they were tracked from 36°C below neck formation to 24°C above it in a total of 17 sequential images according to Table 3.

The analysis in ImageJ software starts by converting the scale of the image into pixels, followed by the conversion of the image into black and white and applying the threshold which matches best the image with the original particles. The ImageJ analysis gives information about particle area, aspect ratio, circularity, Feret diameter, perimeter and roundness.

Particle circularity is a function of particle perimeter, as shown in equation 2. Roundness is a function of particle diameter and equation 3 shows how ImageJ computes it. Equation 4 is used to calculate aspect ratio [36]. The Feret diameter is the average of the diameters captured at every 2 ° of image rotation.

$$Circularity = 4 \times \pi \times \frac{Area}{Perimeter^2} \tag{2}$$

$$Roundness = 4 \times \pi \times \frac{Area}{\pi \times (d_{max})^2} \tag{3}$$

$$AspectRatio = \frac{d_{max}}{d_{min}} \tag{4}$$

2.6. Parameters under discussion at Hot Stage Microscopy

To understand particle coalescence behaviour, this study considered a number of characteristics which can affect the way particles melt and grow, both individually and when in contact with each other. The

first consideration is the methodology used to assess particle and neck growth (Section 2.7); secondly the surface at which the particles are placed, known as substrate, might influence the way they coalesce and their behaviour with temperature increase. Finally, each PEKK grade behaves differently when melting; this difference was quantified in terms of particle shrinkage and neck growth. For each substrate, grade and arrangement (single particle or particles in contact with each other), from five to ten individual particles or necks were analysed. Regarding PEK HP3 grade, no particles were evaluated on PEKK films as the melting temperature of the film is below the T_m of this grade, therefore preventing the visualization of the coalescence for these particles.

2.7. Methods of evaluating particles behaviour with temperature

A few studies were performed on a hot stage platform to evaluate neck, understand particle coalescence and even correlate with the laser sintering process [11, 27, 28, 35]. None of them, however, considered the behaviour of individual particles prior to coalescence. The first stage of this study aims to understand the behaviour of single particles when subjected to heating. This stage attempts to provide enough information to separate physical properties of particles from the sintering process and its mechanisms of diffusion and viscous flow through which consolidation is achieved. This stage also evaluated three different methods of measuring particle dimensions with change in temperature.

The second stage evaluates the length of contact between particles before, at the formation of neck and after it, and correlate with material (viscosity, surface tension) and particle characteristics (size, porosity, morphology, roughness). A great part of this investigation consisted of evaluating the best method to assess and compare particle growth of different grades, considering the particles under analysis. Three different approaches were investigated.

These methods will be discussed in sections 2.7.1 and 2.7.2, respectively, for single particles (methods S) and for neck growth (methods N).

2.7.1. Methods of assessing individual particles behaviour

Method S1:

The first approach selected to analyse individual particles was by evaluating their diameter. As particles are not round, either the longest horizontal diameter (d_h) or the longest vertical diameter (d_v) was measured for the same particle varying with temperature (x), and then divided by its respective initial horizontal or vertical diameter, which is, the diameter measured at room temperature (i) before the start of the test. This method is a rough estimation of particle size as it considers particles as perfect spheres, when in fact they show a quite irregular morphology especially close to room temperature. Equation 5 describes this approach.

$$D = \frac{d_{hx}}{d_{hi}} \quad or \quad D = \frac{d_{vx}}{d_{vi}} \tag{5}$$

D is the final measurement of the particle size, d_{hx} corresponds to the horizontal diameter d_h at a temperature x and d_{hi} is the horizontal diameter of the particle measured at room temperature. In similar way, d_{vx} is the vertical diameter d_v at a temperature x and d_{vi} corresponds to the vertical diameter of the particle measured at room temperature i. A schematic representation of each of these measurements is provided in Figure 3.

Method S2:

The second evaluation consisted of applying the Feret diameter option available (d_f) in ImageJ software. The Feret diameter was measured with the increase in temperature (x) and divided by its respective value at room temperature (i), as shown in Equation 6.

$$D = \frac{d_{fx}}{d_{fi}} \tag{6}$$

d_{fx} is the Feret diameter at a temperature x and d_{fi} is the Feret diameter at room temperature i.

Method S3:

The third approach performed evaluates particle change in terms of perimeter, hence providing a better description of surface texture than Feret diameter analysis. To compare the perimeter values among different grades, the data was also normalized by dividing the perimeter at a respective temperate x (p_x) by the perimeter at room temperature, p_i, as shown in Equation 7.

$$D = \frac{p_x}{p_i} \tag{7}$$

2.7.2. Methods of assessing neck growth (methods N)

Similar approaches were developed to analyse the length of contact (Y) between two adjacent particles with the increase of temperature, also referred as neck when particles are under coalescence. They are described in the following methods.

Method N1:

The first approach consisted of measuring the contact length between the particles with the assistance of the segmented line tool, and then dividing it by the average horizontal or vertical diameter of both particles at the respective temperature under analysis. This approach is described in Equation 8.

$$Y = \frac{y_x}{\frac{d_{1hx} + d_{2hx}}{2}} \quad or \quad Y = \frac{y_x}{\frac{d_{1vx} + d_{2vx}}{2}} \tag{8}$$

In which y_x corresponds to the contact length between two particles at a specific temperature x, d_{1hx} is the horizontal diameter of particle 1 at a temperature x, d_{2hx} is the horizontal diameter of particle 2

at a temperature x, d_{1vx} is the vertical diameter of particle 2 at a temperature x and d_{2vx} is the vertical diameter of particle 2 at a temperature x.

Method N2:

The second approach divides the contact length between the particles by the average Feret diameter of them at a temperature x, according to Equation 9.

$$Y = \frac{y_x}{\frac{d_{1fx} + d_{2fx}}{2}} \tag{9}$$

In which d_{1fx} corresponds to Feret diameter of particle 1 at a temperature x and d_{2fx} is the Feret diameter of particle 2 at a temperature x.

Method N3:

The third approach evaluates the length of contact between two particles in terms of the average perimeter between them, varying with temperature. This approach is described in Equation 10.

$$Y = \frac{y_x}{\frac{p_{x1} + p_{x2}}{2}} \tag{10}$$

In which p_{x1} corresponds to the perimeter of particle 1 at a specific temperature x and p_{x2} is the perimeter of particle 2 at the same temperature x.

3. Results and Discussion

3.1. Scanning Electron Microscopy

The grades were taken to SEM analysis at different magnifications, as shown in Figure 4.

PEK HP3 shows a reasonably regular morphology, the particles are solid and the surface seems smooth at a magnification of 3000x. A few particles resemble a cylinder shape, but most of them approach the spherical shape desired for Laser Sintering. Regarding morphology, the most similar polymer with PEK HP3 is A2, which shows a consistent structure of solid particles with a smooth surface. The other two grades, A1 and B1, present an irregular morphology with pores distributed randomly within each particle individually.

3.2. Particle Size Distribution

The particle size distribution for PAEK grades under analysis are shown in Figure 5. A clear difference is found for A2 grade if compared to the remained PAEK grades; this grade presents an average particle size of 87μm, whilst A1, B1 and HP3 PEK show an average size of, respectively, 53μm, 61μm and 49μm. According to several authors [4, 5], ideal particle size for laser sintering ranges around 60μm with a narrow distribution and a low amount of fine particles at 10μm. Therefore, B1 and A1 grades seem to be more appropriate for Laser Sintering use when considering particle size and distribution.

3.3. Flowability Results

The stability test was slightly modified for each grade, according to the number of cycles necessary to stabilize the powder. A powder becomes stable when the total energy applied by the blade to displace the particles from their original position reaches a plateau. Hence, a total of 20, 20, 40 and 25 cycles were used, respectively, for PEK HP3, A1, A2 and B1. The curves are reported in Figure 6.

Polymer A2 took the longest time to stabilize, reaching a behaviour close to a plateau only around the 26th cycle. For both A1 and B1 grades, the plateau suggesting stability occurred around the 11th cycle, whilst for PEK HP3 such stable behaviour is achieved at the 10th cycle. The standard deviation for each repeat is also significantly greater for A2 than for the other grades; a possible explanation for such behaviour is the larger particle size as well as the density of individual particles of this grade, which requires a higher application of energy to displace the particles at each blade rotation.

By analysing Table 4, none of the SI values are close enough to 1 to consider any of the powders stable. In fact, all the grades took at least a few cycles longer than the standard methodology to finally achieve a plateau; such behaviour is supported by the SI values. Although a plateau is finally reached for all PAEKs, a clear difference is observed for A2 polymer as observed in Figure 6.

The Basic Flowability Energy (BFE) of A2 is significantly higher, followed by PEK HP3. The high BFE for both powders is proportional to their bulk density, and in the case of A2, an effect of particle size too. Interestingly, when normalized against their respective bulk densities, B1 shows the highest BFE, of 525.53 mJml/g, followed by A2 (456.5 mJml/g), A1 (mJml/g) and finally PEK HP3 (422.54 mJml/g). This suggests that cohesivity displays a major role in PEK HP3 but due to the more ideal morphology and density of this powder, such property is softened and does not affect powder flow significantly. On the other hand, porosity seems to display a major role for B1, as well as surface roughness and particle morphology. By analysing SE results, A2 shows the highest values, suggesting particle interlocking but mostly an effect of particle size, as larger particles are harder to be lift than smaller ones. Surprisingly, B1 shows the second highest values of SE, although the standard deviation overlaps the results achieved for PEK HP3. By comparing B1 with A1, both BFE and SE are higher for B1; particle size may be displaying a major role even though CBD difference is almost irrelevant.

3.4. Hot Stage Microscopy for single particles

3.4.1. By Method

Each method described in Section 2.7.1 was firstly compared for A1 particles, following the methodology described in Section 2.5. Figure 7 shows two individual particles of grade A1 at different temperatures.

The particles change in size was assessed using the three different methods presented; the average curves for A1 particles are reported in Figure 8. For the first method, the change in size is not observed at any stage close to the temperature of melting, either for horizontal or vertical measurements: the particles seem

to maintain their size around 10% smaller than their respective size at room temperature, therefore a slight shrinkage is observed before start tracking particle size, at 36 °C below melt. The standard deviation for this method is the highest, as a single measurement of the diameter can vary significantly for non-spherical particles. For the second and third method, the curves show a different trend: at start, their size are just slightly above the initial size, but then shrinkage occurs from 16 °C below the defined temperature of melting. This shrinkage persists until 4 °C above the temperature of sintering, in which particles achieve their minimum size, around 20% smaller than their respective size at room temperature.

Comparing method S2 and S3, the proportion of shrinkage is similar, however method S3 records a particle size 5% smaller than method S2 until (T+16)°C. By considering the irregular morphology presented in Figure 4(2) for grade A1, it is clear that the measurement of the highest diameter, either in the horizontal or vertical direction, is not a good representation of the particle actual size. Indeed this is possibly why shrinkage is notable at lower temperatures than melting - the surface tension of a spherical shape is the lowest and the most stable, therefore an increase in temperature is likely to promote the achieve of a spherical shape by transferring material from the region of maximum diameter to the region of minimum diameter. A single measurement of the diameter is not representative when porous and rough particles such as found in polymer A1 are analysed, hence method S1 is not accurate to measure particle change in size. On the other hand, method S2 and S3 seem to track well the presence of porosity and heterogeneities in the particles and represent better particle behaviour with temperature increase.

3.4.2. By Substrate

Individual particles of grade A1 were tracked on different substrates: glass and glass coated silicone. Silicone was chosen to prevent wettability of the particle with the glass surface. Figure 9 shows the results of the average particle growth of A1 polymer using methods S2 and S3.

Shrinkage is observed for grade A1 just before melting and it progresses for a few degrees after (T)°C. Such shrinkage is clearer especially on glass substrate, in which particle perimeter is reduced by 30% from 12 °C below (T)°C, at (T - 12)°C to 4 °C above (T)°C, at (T + 4)°C, achieving an average perimeter 25% smaller than the original size. When compared with method S2, such reduction is slightly lower: the diameter of individual particles of A1 is reduced by 25% in the same temperature range, and the maximum shrinkage corresponds to a 18% reduction in diameter when compared with the initial particle size.

Both curves on glass substrate are quite clear even after (T + 4)°C, however when on top of glass coated silicone, shrinkage is slightly affected, and the increase in size after (T + 8)°C is not linear as it is on top of glass. The effect of temperature seem to be greater when particles are on top of silicone coated glass, achieving a size 10% larger than the initial size before shrinkage starts at (T-16)°C. From (T-16)°C to (T+4)°C, the particles have their size reduced by 22% for method S2 and 25% for method S3; similar results were achieved for particles on glass.

Both substrates result in similar shrinkage for individual particles of A1 grade, although particles on glass register a higher shrinkage. Such behaviour is expected for these substrates as the silicone prevents wetting of the particles, therefore registering a less significant change in dimension. This is also supported by the fact that particles on silicone were constantly moving on the hot stage platform rather than bound to the glass surface. For this reason, glass substrate was preferred when comparing particle change with temperature for different grades of PAEKs.

3.4.3. By PAEK Grade

Hot Stage Microscopy tests were performed for four different grades on glass substrate using method S3. The results are reported in Figure 10. All PEKKs have shown a shrinkage prior to melting which is not recovered within the range of the analysis but it starts increasing again from (T+4)°C. For B1, particles start to shrink 16 °C before the other grades, showing a less steep shrinkage curve, possibly an effect of its lower viscosity. The authors consider expansion as an increase in particle size from their original state, at room temperature. The particles increase their size but rarely they go beyond their original state, therefore the authors prefer to refer to this as an increase rather than expansion.

From (T+4)°C to (T+24)°C, A1 and PEK HP3 particles increase 15% in average , whilst B1 particles increase 5% and no visible change is observed for A2. As presented in Figure 5, A2 grade shows a larger average particle size distribution, thus to increase surface energy more heat needs to be absorbed. Furthermore, SEM images of these particles show a quite solid structure, hence more energy is required to promote melting. For B1 grade, the effect of temperature increase seems to overlap shrinkage effect; this is supported by the similar particle size of B1 and A1 at (T+20)°C (almost 90% of the original size). All PEKK grades particles do not reach their original size at (T+24)°C, but PEK HP3 expands slightly.

Figure 11 is a representation of change in particle size with temperature for all grades. The same particle had its images overlapped at different temperatures in order to compare the change in size and morphology. As shown by Figure 10, PEK HP3 maintains its size at the end of the test, not changing its morphology greatly as the particle is initially rounder. On the other hand, for particles of PEKK grades, a clear change in morphology is observed especially for A1 and B1, in which the final particle approaches a spherical shape. The size does not seem to change a lot from the initial size at room temperature to the size at T_{max} for any of the grades in the study.

3.5. Hot Stage Microscopy analysis for neck growth

3.5.1. By Method

Studying single particle behaviour during melting aims to help understanding the neck growth process and separating effects associated with the physical behaviour of particles from coalescence. Figure 12 shows

the coalescence process of A1 particles on glass substrate. Different A1 particles in contact with each other were assessed according to the methods presented in Section 2.7.2, the results are shown in Figure 13.

By comparing Figure 13 with Figure 10, a clear correlation is found for particle shrinkage and neck growth: the contact length of particles start to increase significantly when particles begin to shrink, indicating a movement of material to the region of contact between them. Such phenomenon is also observed in Figure 12, in which neck has notably increased with temperature whilst particles are slightly smaller at (T)°C than at room temperature. At this stage, the main transport mechanisms usually present are lattice diffusion, surface diffusion and bulk by bulk diffusion. Neck continues growing after particle shrinkage; viscous flow is now the dominant mechanism of transportation and enables both particles and neck to grow simultaneously [12, 37].

The contact of the particles approach the shape of a logistic curve regardless of the method used. Method N1 seems to be more effective for particle coalescence analysis than for the assessment of individual particle growth, although the average curve for the vertical diameter is not as clear as the others. The curve achieved by dividing the contact length between particles by the average of their Feret diameter (method N2) registers the highest neck growth, with a contact between particles of the same size as their average Feret diameter, hence, full melting and growth. Such behaviour is not as visible for method N3, as perimeter will always be larger than diameter. However, by using method N3, the standard deviation is significantly reduced for any point in the curve. To guarantee the reliability of the test and the consistency with the method used for the assessment of individual particles growth, method N3 was preferred over method N2 and N1.

3.5.2. By Substrate

The process of coalescence for A1 grade was evaluated under three different substrates: glass, glass coated silicone and on PEKK film. The film is made of amorphous PEKK and it aims to replicate the LS process by having a layer of the same material melted under the particles ready to be sintered. The results are presented in Figure 14.

Similar trends are found for A1 on different substrates. When on top of glass coated with silicone, the average neck growth is increased by 15% at (T+24)°C if compared to glass surface, which enables wettability of the particles to occur. Wettability is mitigated in the presence of silicone on glass blades, even though the standard deviation for this substrate is very high and overlaps the values achieved with the particles on glass surface. The results for these two surfaces follow the same trend, but neck seems to start growing earlier on glass than it does on glass coated silicone. Interestingly, particle coalescence on PEKK films have very similar behaviour than on the other two substrates; however, close to melting, the particles suddenly sink on the film and disappear in seconds. This is observed right after (T)°C: at (T+4)°C the particles are already sinking (Figure 15).

The effect of different substrates on neck growth at the start of coalescence can be neglected for PEKK

powders, as similar behaviour is observed for neck growth on PEKK film until it reaches (T)°C. After (T)°C, as the film starts to melt, the particles become quite hard to track. The standard deviation on glass coated silicone substrate is significantly higher than for particles on glass, although the trend is very similar. Hence, the comparison of neck growth among different grades was performed on glass substrate using method N3.

3.5.3. By PAEK Grade

The coalescence process was evaluated for all PAEK grades on glass substrate, according to method N3, and the results are reported in Figure 16. As expected, all PAEK grades show a similar trend and the neck significantly starts to increase from around (T-12)°C. B1 particles showed the highest neck growth from all grades, of approximately 23%, achieving the same final neck growth as A1 and A2 particles. This can be explained by the lower viscosity of B1 grade, which accelerates coalescence rate in addition to particles approaching a spherical shape when close to melt, leading to a significant reduction in perimeter.

All PEKK grades achieved a final neck growth close to 33% at (T+24)°C. Similar trend is observed for PEK HP3, in which neck growth is 28% at (T+24)°C and the rate of coalescence is 16% from (T-36)°C to (T+24)°C. As mentioned in Section 2.1, the melting temperature of PEK HP3 is around 75 °C higher than PEKKs and is closer to the maximum temperature of operation of the hot stage platform. The lower rate of coalescence for this grade can also be explained by the the rounder morphology of the particles at lower temperatures.

Figure 17 shows a schematic representation of the progress of coalescence for all grades. Three images of particles coalescence were overlapped at different temperatures to compare the change in morphology, size and the coalescence progress itself. All particles approach a spherical shape at T_{max}, but this is more significant for A2 and PEK HP3 as their shape are initially more regular and at T_{max} the particles had sufficient time to achieve full melting. The coalescence of A1 draws particles closer, however no expansion is visible at T_{max} as it is observed for B1. The raise in temperature is enough to maintain the initial size of A1 particles by eliminating porosity and surface roughness, however for B1 the particles are significantly expanding from (T)°C and even before that. Such phenomena can be explained by the lower viscosity of this grade in addition to the porosity present, which enables a quicker viscous flow followed by a clear expansion.

For second and third method, all grades on all substrates clearly presented a shrinkage prior to melting. Several studies mention the slow coalescence rate of polymer particles when compared with the predicted rate of mathematical models (Frenkel, Frenkel-Eshelby, Hopper models) to assess coalescence. They attributed that difference to the elastic recovery of particles when heated, at the early stages of neck growth [23–25]. Such phenomenon, however, was not explored experimentally for individual particles before, only in terms of neck growth [22]. The authors believe that shrinkage is delaying the process of coalescence as it draws particles apart at temperatures just below the start of neck growth, continuously acting as a barrier whilst neck is being formed by material flowing to the region of contact between particles. This shrinkage is

possibly caused by the recovery of the elastic deformation before the melt and is supported by the study of individual particles and their melting behaviour presented in Section 3.4.

4. Conclusions

This study investigates different methods of assessing coalescence of particles by using experimental results achieved with PAEK polymers. It aims to compare the effect of melting and sintering performed with the assistance of HSM with the LS process, and hence understand the effect of morphology, size and the rate of these changes with temperature. Three different methods were explored for assessing individual particles growth as well as the coalescence of PAEK particles. Methods S2, N2, S3 and N3 are more accurate as they account for the average of multiple measurements of diameter in each particle (method S2 and N2, Feret diameter) or perimeter (method S3 and N3), resulting in a more reliable analysis. The perimeter method was preferred over Feret diameter method for individual particles and for the analysis of particle coalescence for two main reasons: the reduction in standard deviation and the account for particle texture as well as size in a more accurate manner.

Concerning individual particles behaviour, all PAEK grades shrink prior to melting, and it continues until (T+4)°C. Interestingly, this shrinkage does not seem to be a result of porosity within the particles as all PEKK grades showed similar values of shrinkage. Previous literature associate such behaviour with the recovering of elastic deformation, especially visible for high molecular weight polymers at the early stages of sintering [23, 24].

The study also considered the effect of different substrates on particle growth and coalescence. No significant change in behaviour is observed by using different substrates, in fact all of them showed very similar trends for neck growth. Clearer images were obtained for particles on glass surface, and therefore allowed more accurate measurements during image processing. Particle coalescence on glass coated with silicone presented a slightly higher neck growth, justified by the silicone acting as a barrier for particle wettability with the surface. This substrate seems to slightly delay coalescence and promote a quicker neck growth due to less contact with the surface. Particles on PEKK films with the same T_m were tracked and similar behaviour was found until (T)°C. As expected, the film starts melting at (T)°C and the particles quickly sink in the film, preventing further measurements after (T+4)°C.

PAEK grades were compared on glass surface, using method N3. As Frenkel and other models predicted, viscosity seems to have a significant effect on particle coalescence, supported by comparing the behaviour of A1 and B1 grades. Not only material viscosity but morphology affects particles melting, growth, coalescence and final morphology: more spherical particles seem to promote more spherical coalescence, less porous particles grow in a slower rate as more heat is necessary to promote viscous flow, and the way particles are in contact with each other seem to affect coalescence and growth, although it is complex to measure this

effect with so unique particles. All of these characteristics, however, do not greatly affect neck growth or particle melting, as the trend is quite similar for individual particles and neck of different grades.

The results achieved show a significantly lower rate of coalescence than what predicted by several models discussed in this paper [22]. This is possible a result of shrinkage observed just before melting when evaluating individual particles behaviour, which act against coalescence. This study is a first step to experimentally measure particles growth of different shapes and degrees of porosity and the effect of different substrates on their coalescence. For the first time in literature, Feret diameter and perimeter were used to track and assess neck growth as well as particles growth, and these methods proved to be more effective and reliable. The performance of powder rheology tests support the data provided by the SEM images, PSD and HSM, although it seems that when subjected to higher temperatures, powder characteristics such as morphology, surface texture and porosity are not as significant as their effect at room temperature. This effect is even less visible when particles are placed on PEKK films substrates, the closest simulation able to track particle coalescence and potentially relate with the LS process.

5. Acknowledgements

The authors would like to acknowledge the financial support of Arkema Innovations Chemistry for this study.

6. Data Availability

The raw/processed data required to reproduce these findings cannot be shared at this time as the data also forms part of an ongoing study.

References

[1] L. Verbelen, S. Dadbakhsh, M. Van den Eynde, D. Strobbe, J.-P. Kruth, B. Goderis, P. Van Puyvelde, Analysis of the material properties involved in laser sintering of thermoplastic polyurethane, Additive Manufacturing 15 (2017) 12–19. doi:10.1016/j.addma.2017.03.001.

[2] S. Ziegelmeier, P. Christou, F. Wöllecke, C. Tuck, R. Goodridge, R. Hague, E. Krampe, E. Wintermantel, An experimental study into the effects of bulk and flow behaviour of laser sintering polymer powders on resulting part properties, Journal of Materials Processing Technology 215 (1) (2015) 239–250. doi:10.1016/j.jmatprotec.2014.07.029.

[3] R. D. Goodridge, C. J. Tuck, R. J. M. Hague, Laser sintering of polyamides and other polymers (2012). doi:10.1016/j.pmatsci.2011.04.001.

[4] A. Amado, M. Schmid, G. Levy, K. Wegener, Advances in SLS powder characterization, in: 22nd Annual International Solid Freeform Fabrication Symposium - An Additive Manufacturing Conference, Austin, 2011, pp. 438–452.

[5] S. Yang, J. R. G. Evans, Metering and dispensing of powder; the quest for new solid freeforming techniques, Powder Technology 178 (1) (2007) 56–72. doi:10.1016/j.powtec.2007.04.004.

[6] L. C. Y. Chan, N. W. Page, Particle fractal and load effects on internal friction in powders, Powder Technology 90 (3) (1997) 259–266. doi:10.1016/S0032-5910(96)03228-7.

[7] D. Drummer, D. Rietzel, F. Kühnlein, Development of a characterization approach for the sintering behavior of new thermoplastics for selective laser sintering, Physics Procedia 5 (PART 2) (2010) 533–542. doi:10.1016/j.phpro.2010.08.081.

[8] J. P. Kruth, G. Levy, F. Klocke, T. H. C. Childs, Consolidation phenomena in laser and powder-bed based layered manufacturing, CIRP Annals - Manufacturing Technology 56 (2) (2007) 730–759. doi:10.1016/j.cirp.2007.10.004.

[9] J. Rimell, P. Marquis, Selective laser sintering of ultra high molecular weight polyethylene for clinical applications., Journal of biomedical materials research 53 (4) (2000) 414–420.
URL https://www.ncbi.nlm.nih.gov/pubmed/10898883

[10] N. Hopkinson, R. Hague, P. Dickens, Rapid Manufacturing: An Industrial Revolution for the Digital Age, John Wiley and Sons, Ltd, Chichester, 2005. doi:10.1002/0470033991.

[11] M. Vasquez, N. Hopkinson, B. Haworth, Laser sintering processes: Practical verification of particle coalescence for polyamides and thermoplastic elastomers, Annual Technical Conference - ANTEC, Conference Proceedings 3 (2011) 2458–2462.

[12] J. Kruth, G. Levy, R. Schindel, T. Craeghs, E. Yasa, Consolidation of Polymer Powders by Selective Laser Sintering, in: International Conference on Polymers and Moulds Innovations, 2008, pp. 15–30.

[13] S. Dadbakhsh, L. Verbelen, O. Verkinderen, D. Strobbe, P. Van Puyvelde, J. P. Kruth, Effect of PA12 powder reuse on coalescence behaviour and microstructure of SLS parts, European Polymer Journal 92 (May) (2017) 250–262. doi:10.1016/j.eurpolymj.2017.05.014.

[14] M. Schmid, K. Wegener, Additive Manufacturing: Polymers applicable for laser sintering (LS), Procedia Engineering 149 (June) (2016) 457–464. doi:10.1016/j.proeng.2016.06.692.

[15] B. Haworth, N. Hopkinson, D. J. Hitt, Z. Xiaotao, Shear viscosity measurements on Polyamide-12 polymers for laser sintering, Rapid Prototyping Journal 19 (1) (2013) 28–36. doi:10.1108/13552541311292709.

[16] S. R. Athreya, K. Kalaitzidou, S. Das, Processing and characterization of a carbon black-filled electrically conductive Nylon-12 nanocomposite produced by selective laser sintering, Materials Science and Engineering A 527 (2010) 2637–2642. doi:10.1016/j.msea.2009.12.028.

[17] J. Frenkel, Viscous Flow of Crystalline Bodies Under the Action of Surface Tension, Journal of Physics 9 (5) (1945) 385–391.

[18] J. K. Mackenzie, R. Shuttleworth, A Phenomenological Theory of Sintering, Proceedings of the Physical Society 62 (B) (1949) 833–852.

[19] B. Haworth, N. Hopkinson, D. Hitt, M. Vasquez, Influence of molecular weight and viscosity on particle coalescence for laster sintering of Nylon-12, PPS-27 Polymer Processing Society (2011) 7.1–7.7.

[20] R. W. Hopper, Coalescence of Two Equal Cylinders: Exact Results for Creeping Viscous Plane Flow Driven by Capillarity, Journal of the American Ceramic Society 67 (12) (1984) 262–264. doi:10.1111/j.1151-2916.1984.tb19692.x.

[21] O. Pokluda, C. T. Bellehumeur, J. Machopoulos, Modification of Frenkel' s Model for Sintering, AIChE Journal 43 (12) (1997) 3253–3256. doi:10.1002/aic.690431213.

[22] C. T. Bellehumeur, M. K. Bisaria, J. Vlachopoulos, An Experimental Study and Model Assessment of Polymer Sintering, Polymer Engineering and Science 36 (17) (1996) 2198–2207. doi:10.1002/pen.10617.

[23] S. Mazur, D. J. Plazek, Viscoelastic effects in the coalescence of polymer particles, Progress in Organic Coatings 24 (1-4) (1994) 225–236. doi:10.1016/0033-0655(94)85016-X.

[24] G. C. Kuczynski, B. Neuville, H. P. Toner, Study of sintering of poly(methyl methacrylate), Applied Polymer Science 14 (8) (1970) 2069–2077. doi:https://doi.org/10.1002/app.1970.070140815.

[25] A. Jagota, C. Argento, S. Mazur, Growth of adhesive contacts for Maxwell viscoelastic spheres, Journal of Applied Physics 83 (1) (1998) 250–259. doi:10.1063/1.366679.

[26] C. T. Bellehumeur, M. Kontopoulou, J. Vlachopoulos, The role of viscoelasticity in polymer sintering, Rheologica Acta 37 (3) (1998) 270–278. doi:10.1007/s003970050114.

[27] S. Berretta, Y. Wang, R. Davies, O. R. Ghita, Polymer viscosity, particle coalescence and mechanical performance in high-temperature laser sintering, Journal of Materials Science 51 (10) (2016) 4778–4794. doi:10.1007/s10853-016-9761-6.

[28] G. M. Vasquez, C. E. Majewski, B. Haworth, N. Hopkinson, A targeted material selection process for polymers in laser sintering, Additive Manufacturing 1 (4) (2014) 127–138. doi:10.1016/j.addma.2014.09.003.

[29] A. Barnetson, P. R. Hornsby, Observations on the sintering of ultra-high molecular weight polyethylene (UHMWPE) powders, Journal of Materials Science Letters 14 (2) (1995) 80–84. doi:10.1007/BF00456553.

[30] EOS E-Manufacturing Solutions, EOS PEEK HP3, the high-grade performer (2008).
URL https://webbuilder5.asiannet.com/ftp/2684/sheet_07-08_en_provisional.pdf

[31] Arkema, Kepstan 6000 Series (2013).
URL https://www.arkema.com/export/shared/.content/media/downloads/products-documentations/incubator/arkema-kepstan-6000-tds.pdf

[32] T. Choupin, B. Fayolle, G. Régnier, C. Paris, J. Cinquin, B. Brulé, Isothermal crystallization kinetic modeling of poly(etherketoneketone) (PEKK) copolymer, Polymer 111 (2017) 73–82. doi:10.1016/j.polymer.2017.01.033.

[33] Freeman Technology, About the FT4 Powder Rheometer (2014).
URL http://www.freemantech.co.uk/_powders/ft4-powder-rheometer-universal-powder-tester

[34] O. R. Ghita, E. James, R. Trimble, K. E. Evans, Physico-chemical behaviour of Poly (Ether Ketone) (PEK) in High Temperature Laser Sintering (HT-LS), Journal of Materials Processing Technology 214 (4) (2014) 969–978. doi:10.1016/j.jmatprotec.2013.11.007.

[35] M. Vasquez, B. Haworth, N. Hopkinson, Methods for Quantifying the Stable Sintering Region in Laser Sintered Polyamide-12, Polymer Engineering and Science 53 (6) (2013) 1230 – 1240. arXiv:0406218, doi:10.1002/pen.

[36] T. Ferreira, W. Rasband, ImageJ User Guide IJ 1.46r (2012). arXiv:1081-8693, doi:10.1038/nmeth.2019.

[37] R. Castro, K. van Benthem, Sintering: Mechanisms of Convention Nanodensification and Field Assisted Processes, Springer, New York, 2012.
URL https://books.google.co.uk/books?id=jz11ybvaUo0C&printsec=frontcover#v=onepage&q&f=false

[38] Victrex High Performance Polymers, Victrex HT G22 (2014).
URL https://www.victrex.com/$\sim$/media/datasheets/victrex_tds_ht_g22.pdf

[39] Y. Wang, E. James, O. R. Ghita, Glass bead filled Polyetherketone (PEK) composite by High Temperature Laser Sintering (HT-LS) (2015). doi:10.1016/j.matdes.2015.06.005.

Table 1: General information of PAEK grades in study.

Grade	Viscosity [Pa.s]	T_g [°C]	T_m [°C]
PEK HP3	190[1]	164[2]	372[3]
HL1316[4]	500	160	297
P12S959a[4]	500	160	300
HL1320[4]	300	160	296

[1] [38] Viscosity measured at 400°C according to ISO 11443, values of frequency not provided [2] [39], [3] [30], [4] PEKKs viscosities were measured using a plate rheology equipment operating at 380°C and 1Hz. Values of T_g and T_m were based on DSC results at a rate of 10K/min.

Table 2: Information achieved with Stability and Flow Rate Test [33].

Parameter	Description
Stability Index (SI)	Measures how powder behaviour is preserved through different test conditions. It is an indication of powder uniformity and the presence or not of segregation.
Basic Flowability Energy (BFE)	Measures how difficult to displace the powder using the blade in an unconfined state. It is an indication of powder cohesivity, morphology and packing.
Specific Energy (SE)	Measures how difficult to lift the blade through the powder in an unconfined state. It is an indication of particle size, shape, surface texture, friction and mechanical interlocking.
Conditioned Bulk Density (CBD)	Measures the ability of the powder to fill the voids in the structure without the application of a force. It is an indication of packing efficiency and is directly associated with particle configuration, morphology and flowability.

Table 3: Criteria used to select the images for ImageJ analysis.

1	Room temperature
2	At 200 °C
3	36 °C below neck formation (T-36)°C
4	32 °C below neck formation (T-32)°C
5	28 °C below neck formation (T-28)°C
6	24 °C below neck formation (T-24)°C
7	20 °C below neck formation (T-20)°C
8	16 °C below neck formation (T-16)°C
9	12 °C below neck formation (T-12)°C
10	8 °C below neck formation (T-8)°C
11	4 °C below neck formation (T-4)°C
12	At neck formation (T) °C
13	4 °C above neck formation (T+4)°C
14	8 °C above neck formation (T+8)°C
15	12 °C above neck formation (T+12)°C
16	16 °C above neck formation (T+16)°C
17	20 °C above neck formation (T+20)°C
18	24 °C above neck formation (T+24)°C
19	At maximum experimental temperature
20	At 200 °C, at cooling

Table 4: Summary of Stability and Flow Rate test results.

Grade	*BFE (mJ)*		*SE (mJ/g)*		*SI*		*CBD (g/ml)*	
	Mean	SD*	Mean	SD	Mean	SD	Mean	SD
PEK HP3	226	8	6.24	0.5	1.57	0.1	0.47	0.00
A1	155	9	5.79	0.4	1.48	0.2	0.36	0.00
A2	300	64	7.16	0.2	2.09	2.1	0.50	0.01
B1	183	10	6.41	0.3	1.71	0.3	0.35	0.00

*SD: Standard Deviation.

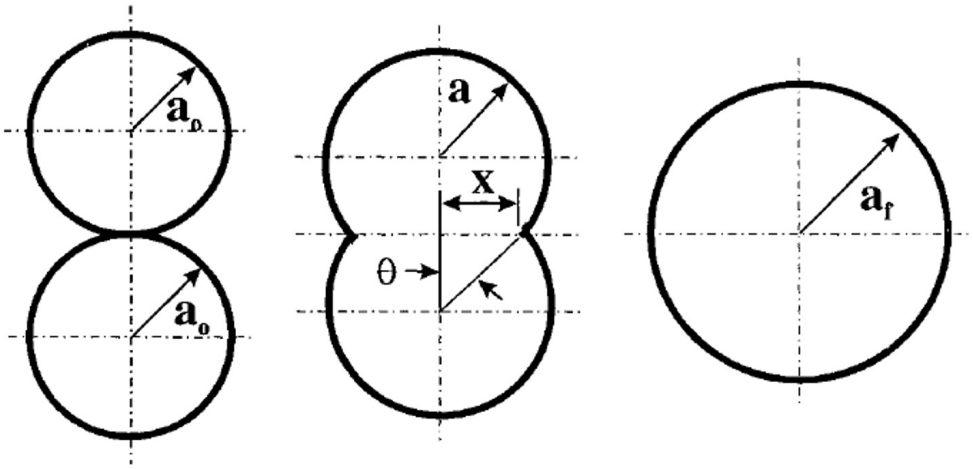

Figure 1: Particle coalescence representation according to Frenkel-Eshelby model [26].

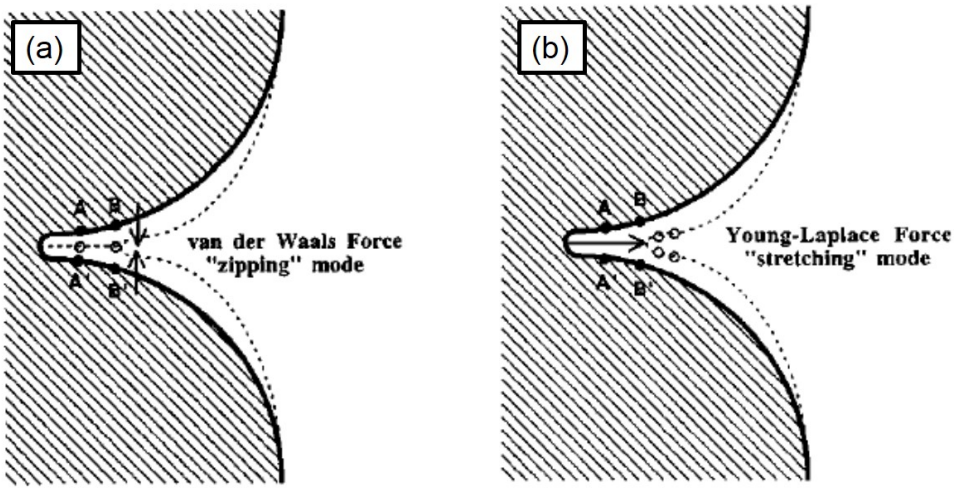

Figure 2: Schematic illustration of contact growth modes according to Jagota et al. [25]. (a) Elastic adhesion driving contact growth in a zipping mode; (b) Tractions viscous sintering driving contact growth in a stretching mode.

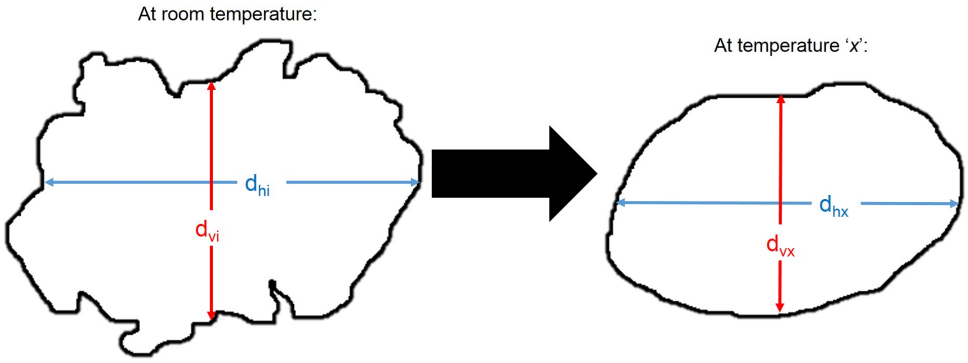

Figure 3: Schematic representation of measurements for method S1.

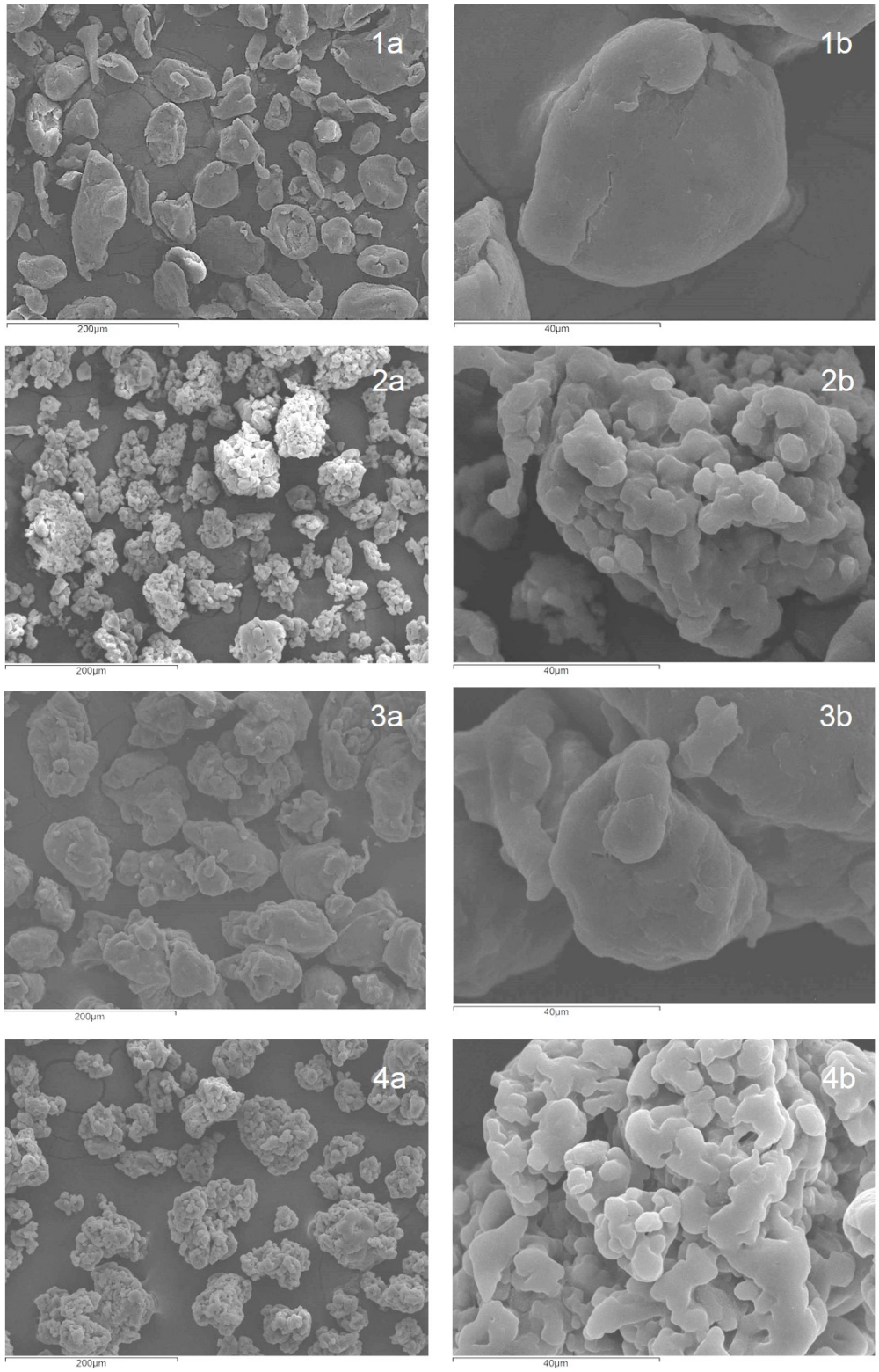

Figure 4: SEM images for different PAEK grades (1-4) at (a) 500x and (b) 3000x of magnification. (1): PEK HP3; (2): A1; (3): A2; (4): B1.

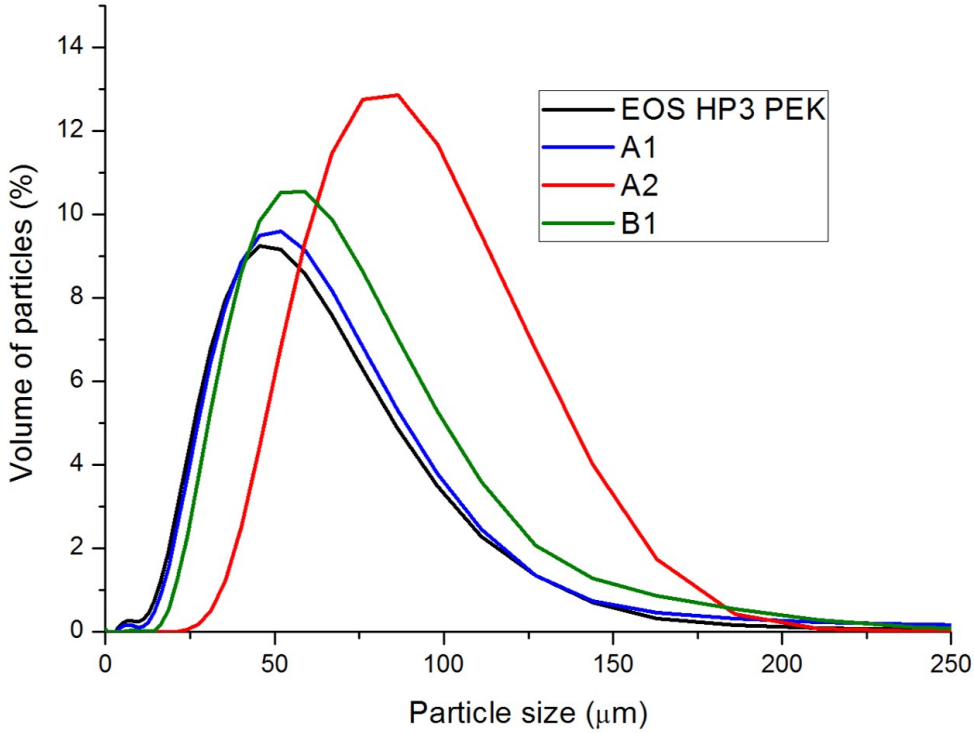

Figure 5: Particle size distribution for different PAEK grades.

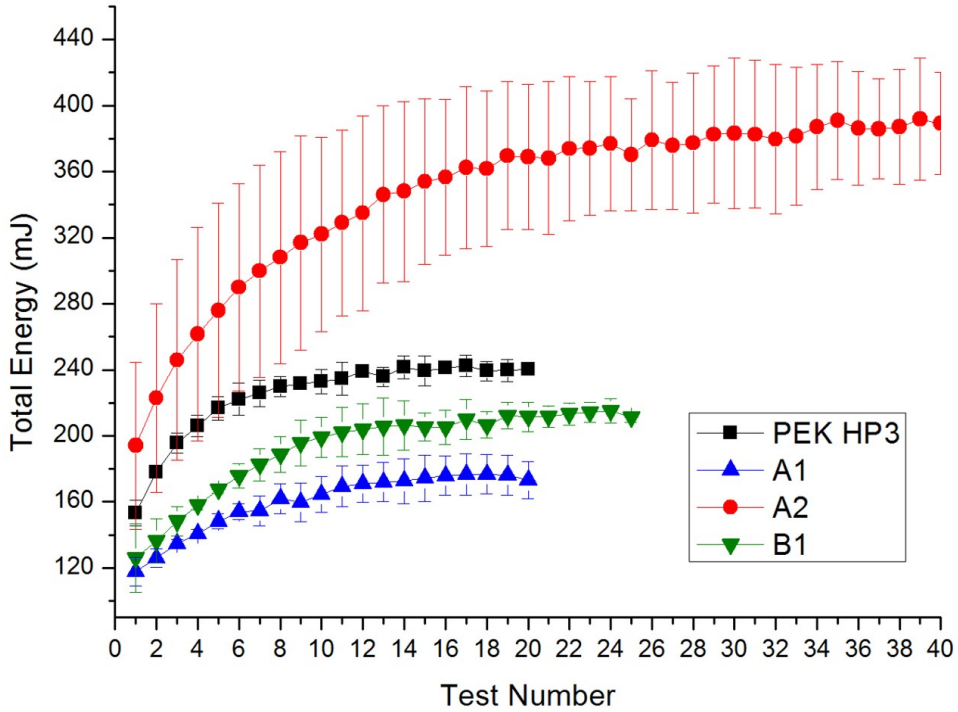

Figure 6: Stability test curves for each PAEK grade.

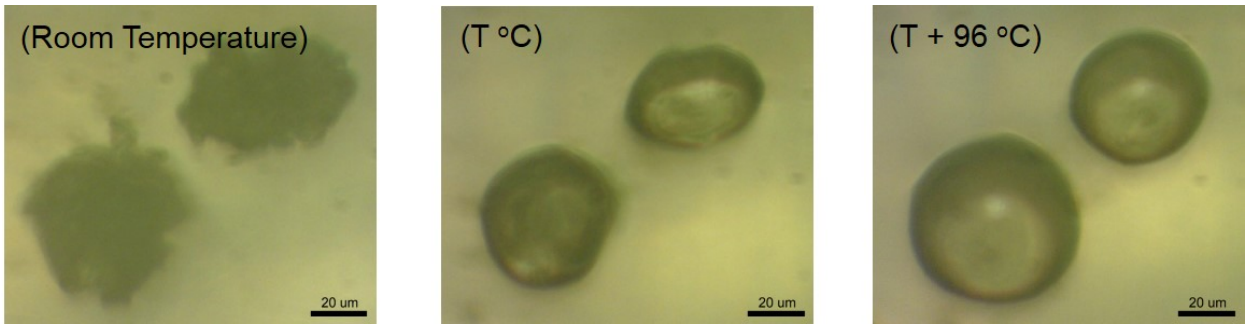

Figure 7: Hot Stage Microscospy images for individual particles of grade A1.

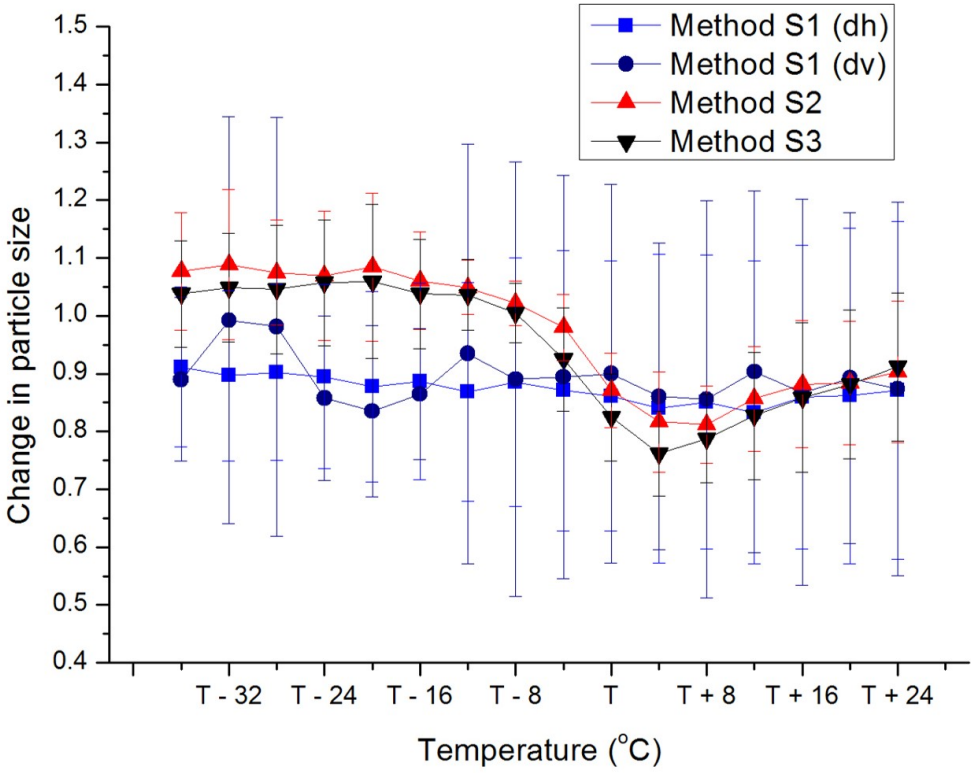

Figure 8: Average change in particle size for A1 on glass substrate, separated by method.

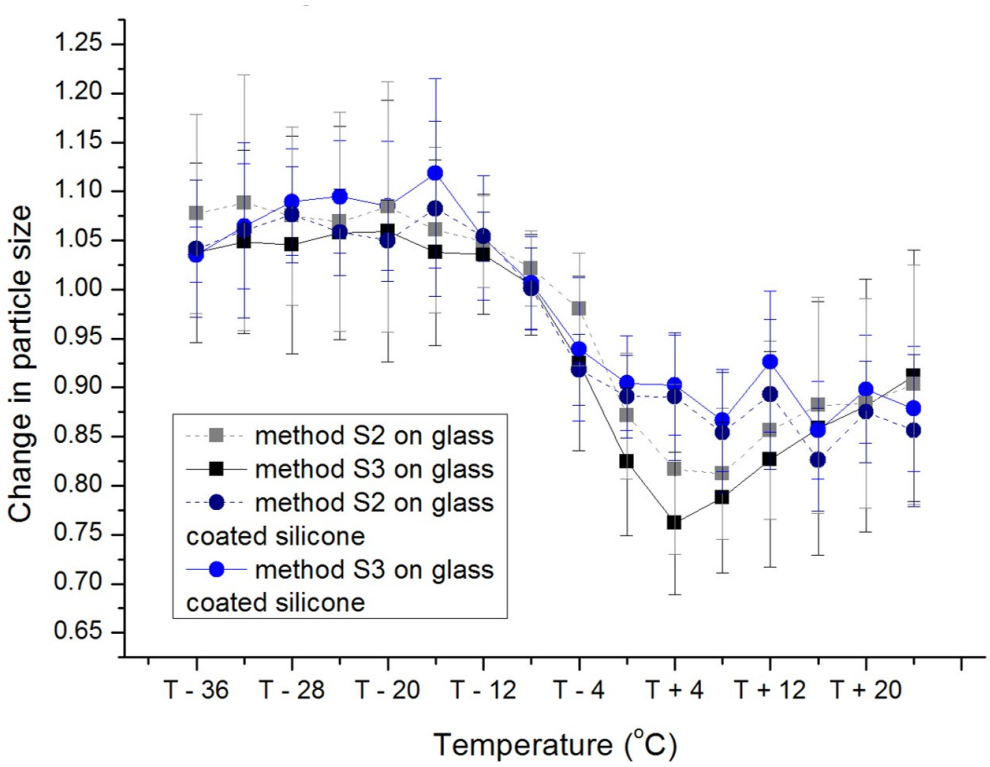

Figure 9: Average Hot Stage Microscopy results for individual particles of A1 on different substrates.

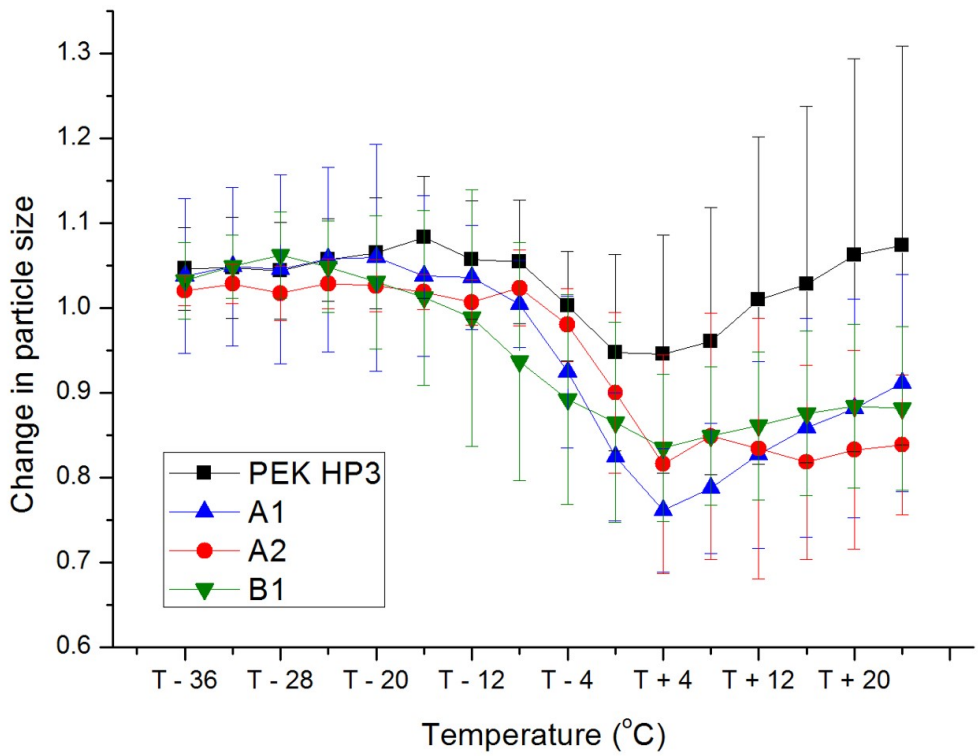

Figure 10: Average Hot Stage Microscopy results for PAEKs grades on glass substrate according to method S3.

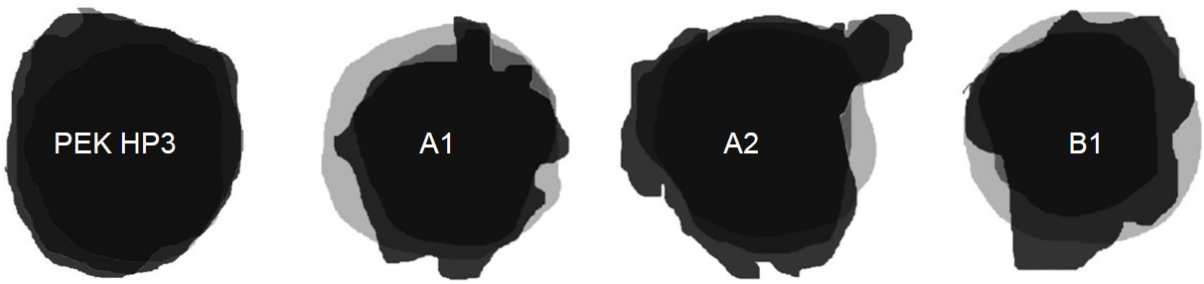

Figure 11: Change in particle size with temperature. The darkest image corresponds to the particle at room temperature, followed by the particle at (T)°C and the lightest colour corresponds to the particle at T_{max}

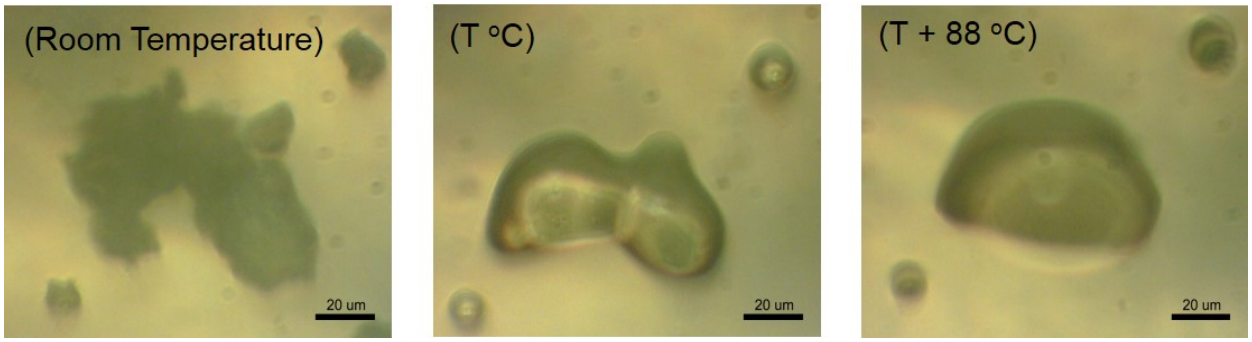

Figure 12: Coalescence of two A1 particles on glass substrate.

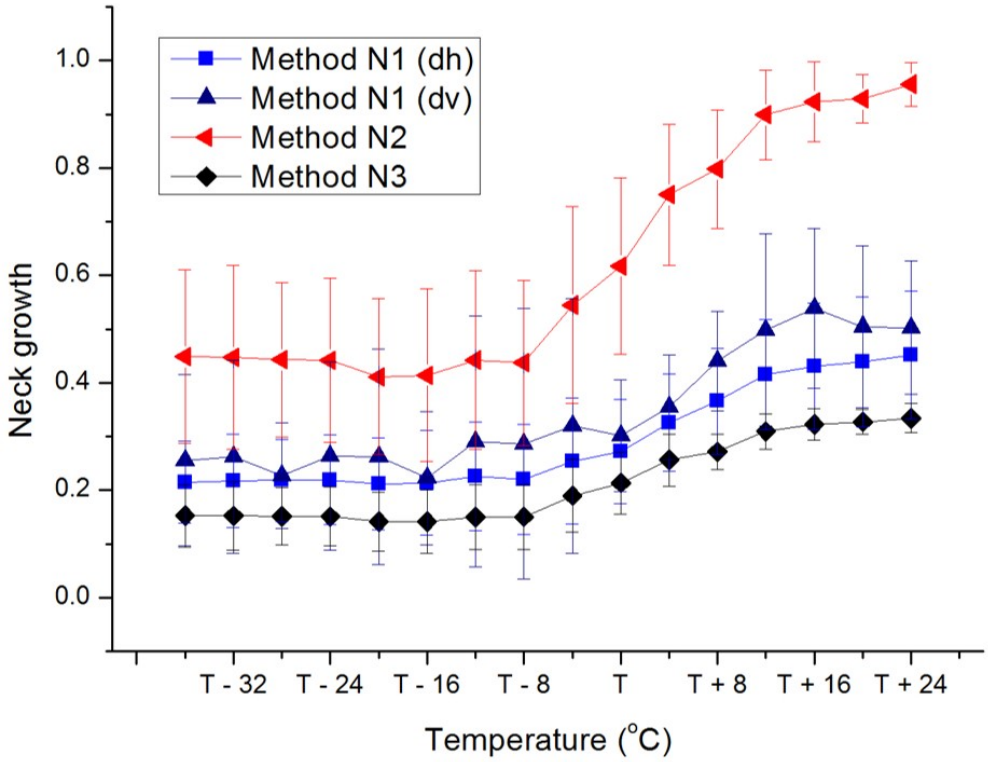

Figure 13: Evaluation of different methods of neck growth analysis for A1 grade on glass.

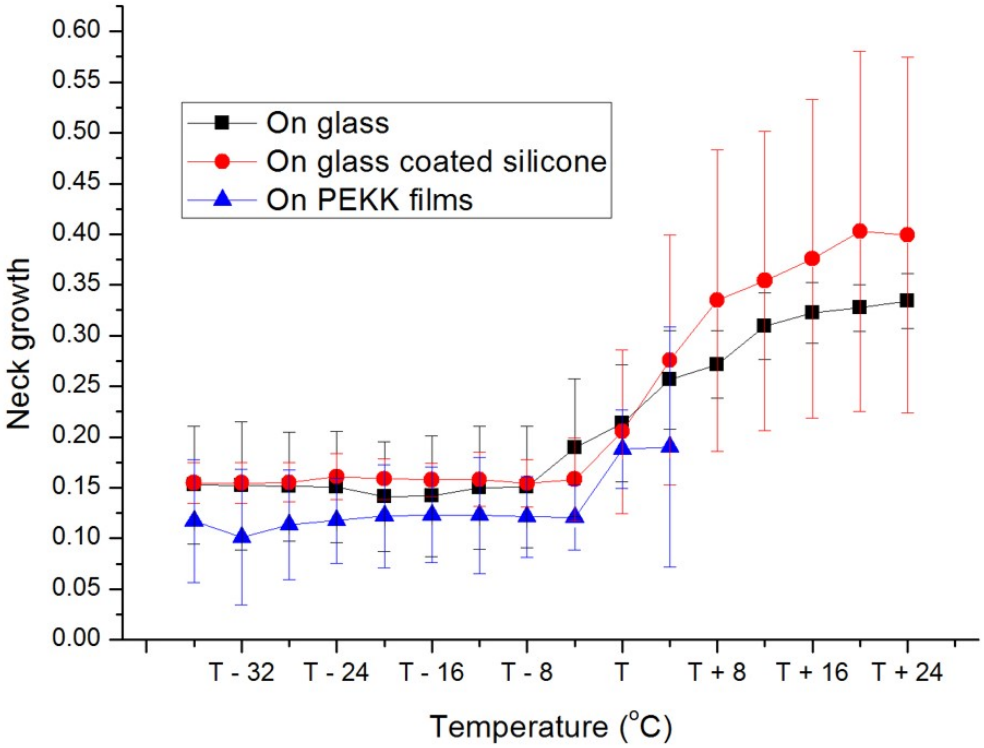

Figure 14: Average neck growth of grade A1 on different substrates using method N3.

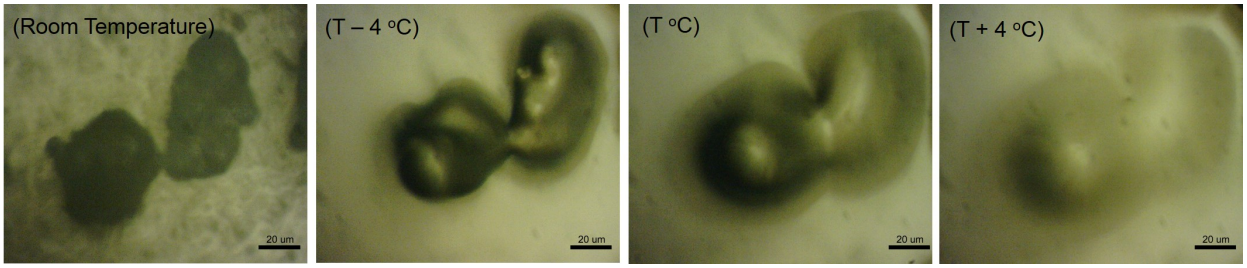

Figure 15: Coalescence of A1 particles on PEKK film.

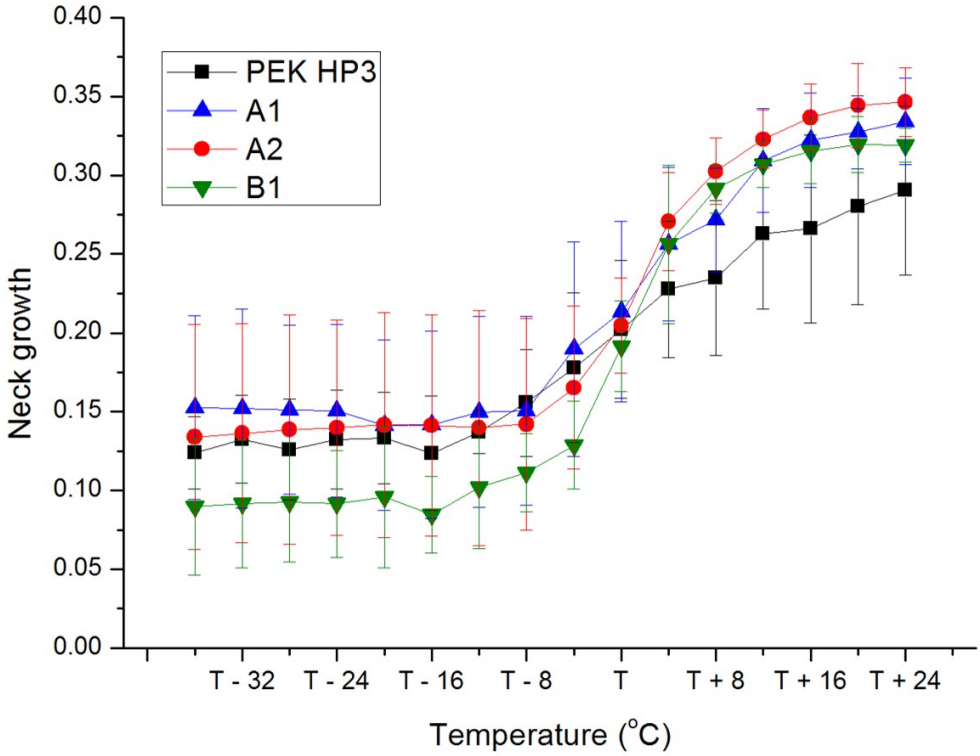

Figure 16: Coalescence of different PAEK grades on glass according to method N3.

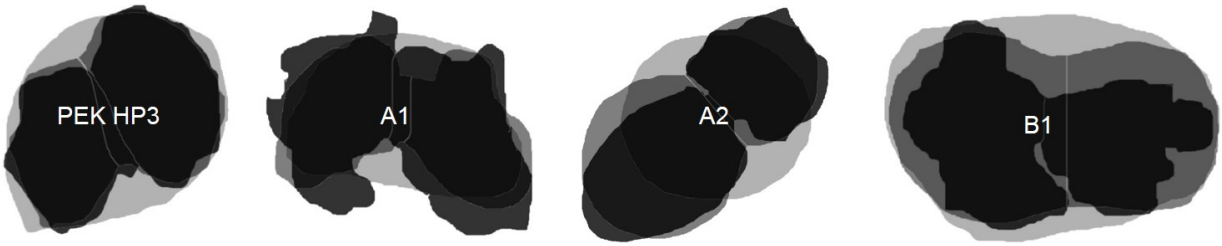

Figure 17: Progress of particles coalescence. The darkest image corresponds to the particles at room temperature, followed by the particles at (T)°C and the lightest colour corresponds to the particles at T_{max}.